Materials Chemistry and Physics 346 (2025) 131318

Contents lists available at ScienceDirect

Materials Chemistry and Physics

journal homepage: www.elsevier.com/locate/matchemphys

Biomolecule encapsulated Ni-doped ZnO quantum dots: A sustainable nanomaterials for antibacterial applications

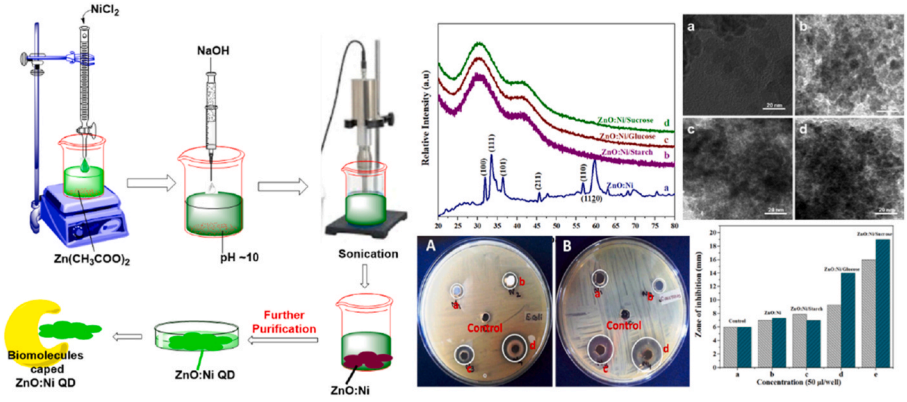
R. Anithadevi [a], J.C. Kannan [b], P. Sangeetha [c], M. Thirumoorthy [d], A. Panneerselvam [e], T. Baranidharan [f], P. Periasamy [g], S. Satheeskumar [h,*]

[a] Department of Chemistry, Eswari Engineering College, Chennai, 600 128, Tamilnadu, India
[b] Department of Physics, K.S.R. College of Engineering, Tiruchengode, 637 215, Tamil Nadu, India
[c] Department of Physics, Sona College of Technology, Salem, 636 005, Tamilnadu, India
[d] Department of Physics, Bannari Amman Institute of Technology, Sathyamangalam, 638 401, Tamil Nadu, India
[e] Department of Physics, Vivekananda College of Engineering for Women (Autonomous), Tiruchengode, 637 205, Namakkal, Tamilnadu, India
[f] Department of Electronics and Communication Engineering, K.S.Rangasamy College of Technology, Tiruchengode, 637 215, Tamil Nadu, India
[g] Department of Physics, Nehru Institute of Engineering and Technology, Coimbatore, Tamil Nadu, India
[h] Centre for Nanoscience and Technology, K.S. Rangasamy College of Technology, Tiruchengode, 637 215, Tamil Nadu, India

HIGHLIGHTS

- Green precipitation method with optimized temperature, reaction times and pH was adopted to prepare pure ZnO, Ni-doped ZnO and biomolecule-capped Ni-doped ZnO quantum dots (QDs).
- Ni doping and biomolecule capping (starch, glucose, sucrose) combinations led to the enhanced stability of the QDs, excellent dispersion, tunable bandgap, and excellent optical properties.
- The antibacterial tests against gram-negative (E. coli) and gram-positive (S. aureus) bacteria demonstrated superiority in antibacterial activity.
- The enhancement of the antibacterial effect is elucidated by more reactive oxygen species (ROS) production, the efficient disruption of the membrane, the decreased size of particles, as well as the stable encapsulation of biomolecules.

GRAPHICAL ABSTRACT



ARTICLE INFO

Keywords:
Quantum dots
Zinc oxide
Nickel
Bio-molecules
Anti-bacterial activities

ABSTRACT

Here, pure ZnO, nickel (Ni) doped ZnO, and biomolecule-capped ZnO quantum dots (QDs) have been synthesized using an eco-friendly green synthesis approach with optimized conditions (temperature, reaction time, and pH). The structure of ZnO quantum dots (QDs) with nickel (NiII) dopant was investigated using XRD, and a mixed cubic-hexagonal crystal structure with an average crystallite size of 12 nm was obtained. The transmission electron microscopy (TEM) images showed spherical morphology with average particle sizes below 10 nm, and

* Corresponding author.
E-mail address: satheesphysics@gmail.com (S. Satheeskumar).

https://doi.org/10.1016/j.matchemphys.2025.131318
Received 17 April 2025; Received in revised form 11 July 2025; Accepted 16 July 2025
Available online 18 July 2025
0254-0584/© 2025 Elsevier B.V. All rights are reserved, including those for text and data mining, AI training, and similar technologies.

the particles were uniformly dispersed in the biomolecule matrix. A red shift of an absorbed spectrum peak was observed at ~343 nm due to the sp-d exchange interactions between the Ni^{2+} ions and the electrons on the host lattice of the ZnO. Firm violet-blue emission peaks associated with near-band edge excitonic recombination and trap state emissions were observed from biomolecule capping, which was confirmed by the photoluminescence (PL) spectra. The antibacterial activities of the synthesized QDs were tested against gram-negative (E. coli) and gram-positive (S. aureus) bacteria using the disc diffusion method. Sucrose-capped nickel-doped QDs (ZnO:Ni/Sucrose) showed the best antibacterial activities. Considerably larger inhibition zones were achieved for these samples compared to starch and glucose-capped samples. Increased generation of reactive oxygen species (ROS) coupled with disruption of the bacterial membrane accounts for the observed superior antibacterial effect from the capped particles aided by reduced size. This work proposes a novel, economically favorable, and ecologically friendly method for fabricating biomolecule-stabilized Ni-doped ZnO QDs with notable antibacterial activity. These results demonstrate that ZnO:Ni/Sucrose QDs are viable options for biomedical fields focused on fighting against microbial infections.

1. Introduction

The unique physicochemical properties of ZnO (Zinc Oxide) nanostructures, including a wide bandgap of 3.37 eV, a high exciton binding energy of 60 meV, and outstanding optical, electrical, and antibacterial qualities, have drawn significant attention [1]. These features enable the researchers to use ZnO in photocatalysis, biomedicine, and optoelectronics [2]. However, the potential of ZnO quantum dots (QDs) is severely restricted by challenges related to particle agglomeration, low stability in aqueous environments, and suboptimal antibacterial activity [3]. Introducing defect states through doping with transition metals, such as nickel (Ni), has significantly enhanced ZnO's optical and electronic properties. Furthermore, modifying the surface with biomolecules as capping agents has emerged as a green method for functionalization and improved stability of the particles [4]. Studies indicate that doping Zinc Oxide (ZnO) with nickel reduces surface roughness, enhances surface quality, and tunes the electrical bandgap through sp-d exchange interactions between Ni^{2+} ions and the electrons of the ZnO lattice [5]. These enhancements can increase light absorption and charge separation efficiency, suggesting that Ni-doped ZnO could benefit photocatalytic and antibacterial applications [6]. Capping with biomolecules stabilizes ZnO quantum dots (QDs) by preventing agglomeration and introducing functional groups into the biological system, and capping agents such as starch, glucose, and sucrose appeal due to their non-toxic and biodegradable nature and ability to function as reducing and stabilizing agents during synthesis [7]. These biomolecules provide additional active sites that may enhance the production of reactive oxygen species (ROS), which is a crucial mechanism behind the antibacterial activity of ZnO QDs [8].

Despite several progress, detailed studies remain lacking in evaluating the structural, optical, and antibacterial properties of ZnO QDs about the effects of Ni doping and biomolecule capping [9]. Most existing literature focuses on either doping or capping processes in isolation, leading to a gap in understanding how these two approaches interactively influence material performance. For instance, although it is recognized that Ni-doped ZnO suffers less from recombination loss of photo-generated electron-hole pairs, the impact of biomolecule capping on further enhancing these properties remains largely unexplored. Similarly, while biomolecule-capped ZnO QDs are known to be more stable and biocompatible, their role in doped systems is still poorly understood [10]. The intrinsic antibacterial properties of ZnO NPs stem from their ability to produce reactive oxygen species (ROS), release Zn^{2+} ions that damage bacterial membranes, and electrostatically interact with negatively charged bacterial surfaces. While having inherent antibacterial traits, ZnO NPs have difficulties with particle agglomeration, low stability in aqueous suspensions, and poor antibacterial activity [11]. Other researchers have sought to improve the antibacterial functions by using transition metal dopants, biomolecule capping, and hybridization with other nanomaterials.

The transition element doping modifies the electronic structure of ZnO by creating defect states that facilitate ROS generation. This is particularly effective in Ni doping due to the close ionic radii of Ni^{2+} (0.69 Å) and Zn^{2+} (0.74 Å), allowing for substitution in the ZnO lattice with minimal distortion [12]. Enhanced antibacterial activity of Ni-doped ZnO against Escherichia coli (E. coli) and Staphylococcus aureus (S. aureus) infections has been recorded. This is explained by the increased ROS production and enhanced charge separation efficiency [13]. It has also been noted that other dopants, Fe^{3+}, Mn^{2+}, and $Co^{2,+}$ have been equally effective in improving antibacterial activity for the same reasons. Starch, glucose, and sucrose are natural biomolecules that serve as nontoxic caps that stabilize ZnO NPs from agglomeration while introducing functional biomolecules that enhance biological interaction [14]. Compared to the uncapped counterparts, biomolecule-capped ZnO NPs exhibit improved dispersion and reduced particle size, resulting in higher ROS generation and superior antibacterial activity [11]. Sucrose-capped Ni-doped ZnO quantum dots (QDs) are remarkable bacteria against E. coli and S. aureus due to their smaller particle size (~10 nm) and stable biomolecule encapsulation [1].

The combination of ZnO with other metal oxides or carbon materials creates synergistic benefits that improve its antibacterial activity: the ZnO–Ag hybrids take advantage of the ROS generation potential of ZnO as well as the silver ion release from Ag nanoparticles for excellent bactericidal effects against antibiotic-resistant strains [15], CNT/ZnO composites take advantage of the mechanical disruption of the CNTs membranes and the oxidative damage by the ROS from ZnO [16], Graphene oxide (GO)/ZnO hybrids have superior antibacterial activity because of the oxidative stress induced by ZnO while GO physically ruptures bacterial membranes due to its sharp edges ("nanoscalpel") [17], MXene/ZnO composites take advantage of the ability of MXene nanosheets to cause membrane damage and the generation of ROS from ZnO [18]. Although notable strides have been made in improving the antibacterial activities of ZnO nanostructures using doping, capping, and hybridization methods, few attempts have been made to create a combined study that looks at the effects of the combined approaches [19]; many other investigations center on particular approaches without thoroughly examining their interactions with one another. The current work uses the green synthesis approach to produce pure ZnO QDs, Ni-doped ZnO QDs, and biomolecule-capped Ni-doped ZnO QDs. It is the first work that shows a systematic synthesis of transition metal (Ni) doped whilst capping with natural biomolecules (starch, glucose, sucrose) ZnO quantum dots thus allowing a direct comparison of the synergistic effects of such combinations of structure, optical and antibacterial activity. We show that the dual strategy it produces very stable, dispersible and biocompatible QDs with highly tunable band gaps and significantly improved antibacterial effect, in particular, in the case of sucrose-capped samples, which is due to the elevated ROS production and disruption of membranes. Being sustainable and scalable, the new method gives new perspectives on defect engineering and surface functionalization that can form a multifunctional platform of advanced biomedical applications. The structural, morphological, optical, and antibacterial characteristics of the QDs will be analyzed in detail to examine the effects of the combined doping and biomolecule capping.

The findings of this study are expected to contribute to the improved design of multifunctional nanomaterials for biomedical applications.

Material Type	Example Materials	Antibacterial Mechanisms	Enhanced Antibacterial Activity Against	References
Pure & Doped ZnO	Ni-doped ZnO, Fe-doped ZnO	ROS generation, ion release, membrane disruption	E. coli, S. aureus, P. aeruginosa	[20]
Biomolecule-Capped ZnO	Glucose-, Sucrose-capped Ni–ZnO	Improved stability, reduced size, enhanced ROS	E. coli, S. aureus	[1]
Metal Oxide Hybrids	ZnO–TiO_2, ZnO–Ag, ZnO–CuO	Synergistic ROS production; metal ion release	Antibiotic-resistant strains; broad-spectrum	[21]
CNT/ZnO Hybrids	CNT/ZnO composites	Physical disruption; oxidative stress	Broad-spectrum pathogens	[16,22]
Graphene-Based Hybrids	GO/ZnO, rGO/ZnO	Nano-knives effect; wrapping/ trapping bacteria; enhanced ROS	Broad-spectrum pathogens (E. coli, S.aureus)	[23,24]
MXene/ZnO Hybrids	$Ti_3C_2T_x$ MXene/ZnO	Sharp-edge physical damage; oxidative stress	Broad-spectrum pathogens (E. coli, B.subtilis)	[25]

2. Experimental technique

2.1. Materials and method

Analytical-grade zinc acetate dihydrate [$Zn(CH_3COO)_2{\cdot}2H_2O$], nickel chloride hexahydrate ($NiCl_2{\cdot}6H_2O$), sodium hydroxide (NaOH), starch, glucose, and sucrose were purchased from Merck Chemicals in Mumbai, India. All solution preparations utilized double-distilled water.

2.2. Synthesis of ZnO quantum dots

2.2.1. Synthesis of pure zinc oxide quantum dots

Quantum dots (QDs) are usually synthesized using the two-step approach, as shown in Fig. 1. A modified green precipitation technique was used to synthesize pure ZnO QDs. It begins with preparing 0.1 M Zinc Acetate Dihydrate in deionized double distilled water at room temperature while stirring continuously. Next, freshly prepared NaOH solution was added using a drop funnel until the pH of the solution was 10. The mixture was then left under continuous stirring for 4 h, during which a white precipitate was formed. The precipitate was harvested and thoroughly washed using DDW to remove residual ions and then dried in a vacuum desiccator. Finally, the dry powder was placed in an oven set to 400°C for 2 h, which completed the transformation of Zinc Hydroxide [$Zn(OH)_2$] into crystalline Zinc Oxide (ZnO) QDs.

2.2.2. Synthesis of Ni-doped ZnO QDs

The Ni-doped ZnO QDs were synthesized by incorporating Ni into the ZnO lattice. A 0.1 M solution of Zinc acetate dihydrate was dissolved in double distilled water while stirring. Nickel chloride hexahydrate was added to the solution in stoichiometric amounts until the solution obtained a pale green color, which indicates that Ni^{2+} ions were present in the solution. The pH of the solution was adjusted to 10 and was followed by vigorous stirring for 4 h. The resulting dark green colloidal solution was then sonicated for 30 min to help stabilize the dispersion of the particles. The precipitate was centrifuged at 10000 rpm for 30 min, washed with double distilled water, vacuum desiccated, and annealed at 400 °C for 2 h.



Fig. 1. Schematic representation of Biomolecules caped ZnO: Ni QD.

2.2.3. Synthesis of biomolecule-capped Ni-doped ZnO QDs

Biomolecule-capped Ni-doped ZnO QDs were fabricated by first dropping a specific quantity of starch, glucose, or sucrose into double distilled water (DDW). The mixture was gradually poured into the zinc acetate-nickel chloride solution while controlling the temperature to a pH of 10. During the subsequent 4 h of vigorous stirring, the solution turned into a brownish colloidal solution, showing the biomolecule encapsulation on the surface of ZnO:Ni. Ultrasonication at room temperature at ambient pressure was performed for 30 min. After that, the colloid underwent centrifugation at 10,000 rpm for 30 min, followed by washing with DDW, drying under a vacuum, and annealing at 400 °C.

2.2.4. Antibacterial activity

The antibacterial activity of the synthesized quantum dots (QDs) was tested against the Gram-Negative E. coli and Gram-Positive S. aureus using the disc diffusion method. For this method, Muller-Hinton agar plates were made and inoculated by the bacterial strains cultured in nutrient broth at 35° ± 2° for 24 h. Sterile discs with different QD samples (ZnO:Ni/Starch, ZnO:Ni/Glucose, ZnO:Ni/Sucrose) were added to the agar plates and positive controls where DMSO was treated on the discs. The plates were incubated at 35° ± 2° for 24 h, and the antibacterial activity was measured by quantifying inhibition zones using calipers after removing discs.

2.2.5. Instrumentation

The following instruments were used for sample characterization. A Bruker D8 Advance X-ray diffractometer with Cu Kα radiation was used (λ = 1.5406 Å) for structural analysis. The data was collected over the 2Θ range of 20°–80° with a rate of 0.02°/s. JEOL JEM-2100 TEM with 200 kV accelerating voltage was used for the morphologic study. The particles were sized and shaped based on the examined TEM pictures. Band gap energy was calculated from the optical absorption spectrum taken with JASCO V-670 UV–Vis spectrophotometer (200–800 nm). The PL emission spectrum was taken with in-orbiting xenon flame utilizing Horiba Jobin Yvon Fluoromax-4 spectrofluorometer as the excitation source.

3. Result and discussion

3.1. XRD structural analysis

The X-ray diffraction (XRD) analysis of pure zinc oxide (ZnO), nickel-doped zinc oxide (ZnO: Ni), and biomolecule-capped Ni-doped quantum dots (bionanocomposites) ZnO: Ni/Starch, ZnO: Ni/Glucose, ZnO: Ni/Sucrose is presented. The distinct peaks indicative of the crystalline phases from the synthesized samples are shown in Fig. 2 within the diffraction patterns. The XRD patterns illustrate that the ZnO: Ni QDs exhibit a mixed cubic-hexagonal crystal structure. The {100}, {002}, and {101} peak planes correspond to the hexagonal wurtzite structure of ZnO (JCPDS card No. 36–1451), along with the cubic phases resulting from the Ni doping [26]. A change in the intensity of the peaks with increasing 2θ confirms that the Ni doping caused lattice distortion due to the substitutional incorporation of Ni^{2+} ions into the ZnO lattice. The distortion caused by Ni arises from the reorganization of the crystal lattice, as the ionic radius of Ni^{2+} (0.69 Å) is smaller than that of Zn^{2+} (0.74 Å) [27]. The biomolecules encapsulating crystalline ZnO: Ni QDs resulted in the broadening of the sharp diffraction peaks, attributed to their amorphous nature [28]. This observation applies to polymer or other biomolecule-coated nanoparticles. The weak peaks within the amorphous matrix confirm that the ZnO: Ni QDs maintain a crystalline nature despite the suppression [2].

The average crystallite size of ZnO: Ni QDs was determined using the Debye-Scherrer equation [29] as follows: $D = k\lambda/(\beta\cos\theta)$ and provide in Table .1.

Where D denotes crystallite size, k is the Scherrer constant (k = 0.9), λ is the wavelength of Cu-Kα radiation (λ = 1.5406 Å), β is the full width at half maximum (FWHM) of the diffraction peak, θ is the Bragg angle.

The estimated crystallite size for ZnO: Ni QDs was around 12 nm. However, calculating the particle size of biomolecule-capped samples proved challenging due to the increased broadening of peaks resulting from surface encapsulation. Previous literature indicates broad peaks suggest particle sizes within the 10–20 nm range [1]. The broadening and suppression of the diffraction peaks for biomolecule-capped samples indicate a strong interaction with ZnO: Ni QDs and capping agents starch, glucose, and sucrose, which may lead to lower crystallinity and higher dispersion within the biomolecular matrix. This has been observed in other studies involving polymer or biomolecule-capped nanoparticles [30]. The lattice parameters (a and c) for ZnO: Ni QDs were calculated using Bragg's law and compared with standard values for pure ZnO. Alterations in the lattice constants associated with incorporating Ni^{2+} ions are attributed to internal compressive stress caused by doping. This stress can increase defect density, which is crucial for enhancing the optical and antibacterial activity of the material [31].

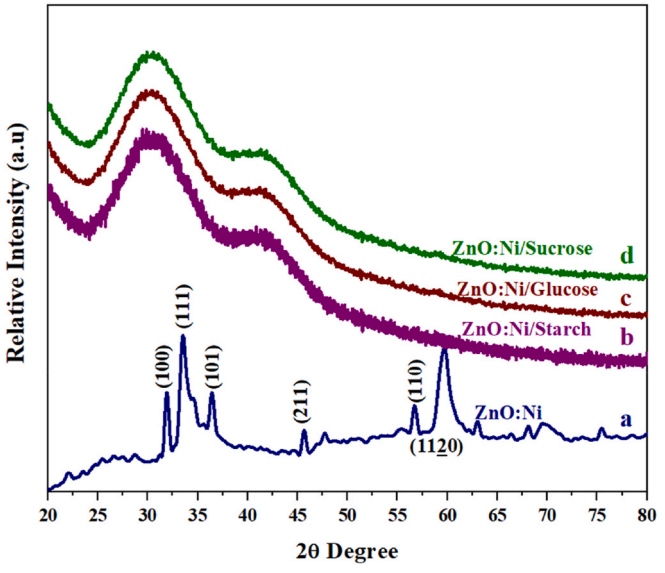


Fig. 2. XRD patterns of (a) ZnO: Ni, (b) ZnO: Ni/Starch, (c) ZnO: Ni/Glucose and (d) ZnO: Ni/Sucrose QD samples.

Table 1
XRD analysis Results of ZnO:Ni Nanostructures.

2θ (°)	Plane	θ (°)	FWHM (°)	Crystallite Size (nm)	Micro-strain (ε)	Dislocation Density (nm^{-2})
31.8	(100)	15.9	0.2	41.3	$3.06 \times {}^{-3}$	$5.86 \times {}^{-4}$
34.5	(101)	17.25	0.2	41.59	$2.81 \times {}^{-3}$	$5.78 \times {}^{-4}$
36.2	(111)	18.1	0.2	41.79	$2.67 \times {}^{-3}$	$5.73 \times {}^{-4}$
47.5	(211)	23.75	0.2	43.4	$1.98 \times {}^{-3}$	$5.31 \times {}^{-4}$
56.6	(110)	28.3	0.2	45.11	$1.62 \times {}^{-3}$	$4.91 \times {}^{-4}$

Table 2
Comparison of bacterial killing effect (Zone of inhibition) after 24 h.

Sample (QD)	Control (mm)	Zone of inhibition (mm)	
		E. coli	S. aureus
DMSO	6	6	6
ZnO:Ni	6	7	7.3
ZnO:Ni/Starch	6	7.9	7.4
ZnO:Ni/Glucose	6	9.2	14
ZnO:Ni/Sucrose	6	16	19

3.2. TEM morphology analysis

In analyzing the surface morphology, particle size, and dispersion of the resulting quantum dots (QDs), which include pure ZnO, Ni-doped ZnO (ZnO: Ni), and biomolecule-capped Ni-doped ZnO QDs (starch, glucose, and sucrose), Transmission Electron Microscopy (TEM) was conducted and displayed in Fig. 3 selected micrographs. The TEM images of ZnO: Ni QDs showed nanoparticles in a spherical shape with average particle sizes ranging from 8 to 10 nm. These particles displayed dispersive uniformity without considerable agglomeration, suggesting effective stabilization during synthesis. The spherical morphology has also been established and reported in studies on transition metal-doped ZnO nanoparticles synthesized through greener methods. Unlike the previously discussed class of QDs, biomolecule-capped Ni-doped ZnO QDs exhibited clouds of particles in a spherical shape [32]. However, the particles were encapsulated within an amorphous biomolecular matrix, causing them to cluster due to interactions between the capping agents and the surfaces of the nanoparticles [33]. These capping agents, in the form of starch, glucose, or sucrose, enhance the dispersion and stabilization of the nanoparticles, suppressing aggregation. This clustering morphology is particularly noteworthy as it indicates strong encapsulation effects that would be observed for nanoparticles in biological environments [14].

The polymeric characteristics of starch, glucose, and sucrose biomolecules can explain the clustering effect of biomolecule-capped QDs. These biomolecules stabilize by encapsulating the nanoparticles within protective layers formed through hydrogen bonds and electrostatic forces. Encapsulation enhances interaction with bacterial membranes during antibacterial activity, prevents agglomeration, and increases biocompatibility [34]. Due to the surface biomolecules, the average particle size for biomolecule-capped QDs was approximately 10–15 nm, more significant than that of uncapped ZnO: Ni QDs. This aligns with

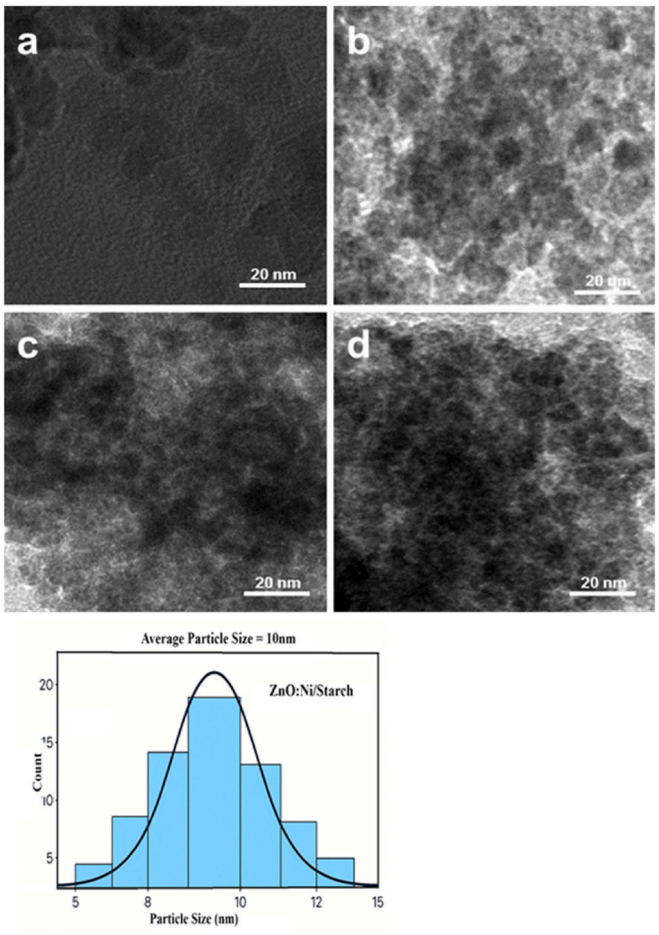


Fig. 3. TEM micrograph of (a) ZnO:Ni, (b) ZnO:Ni/Starch, (c) ZnO:Ni/Glucose and (d) ZnO:Ni/Sucrose QD samples.

earlier findings where blends of constituents' natural polymers from renewable resources were utilized as capping agents for metal oxide nanoparticles. The spherical shapes and larger particle sizes observed in this study are similar to the observations made on Ni-doped ZnO nanoparticles synthesized using green methods [35]. It has been proven that the stability and resistance to particle aggregation in similar systems with biomolecule capping are superior. Moreover, the noted clustering tendency here was also recorded for polymer-capped nanoparticles reported for use in biomedicine. The XRD peak shifts and intensity changes in Ni doped ZnO show that lattice distortion and defect formation have taken place in Ni doped ZnO. Further capping of the biomolecules (starch, glucose, sucrose) still further broadens and suppresses XRD peaks and gives somewhat larger particles in dispersion (TEM) because of the diminished crystallinity and enhanced surface effects. Therefore, Ni substitution and encapsulation of biomolecules take a synergetic contribution in altering the structural, morphologic, and structural stability of ZnO QDs, leading to increased dispersion and clear functional characteristics.

3.3. Optical analysis

The optical characterizations of pure ZnO, Ni-doped ZnO (ZnO: Ni), and biomolecule-capped Ni-doped ZnO quantum dots (ZnO: Ni/Starch, ZnO: Ni/Glucose, ZnO: Ni/Sucrose) were conducted using UV–Vis spectroscopy along with photoluminescence (PL) techniques [36]. These analyses provide insights into the evaluated quantum dots (QDs), including their bandgap energy, absorption characteristics, and emission profiles. The UV–Vis absorption spectra of all samples are summarized in Fig. 4. The absorption peak for ZnO: Ni QDs was around 343 nm, which is red-shifted compared to pure ZnO QDs [37]. This red-shift is explained by sp-d exchange interactions between the band electrons and the localized d-electrons of Ni^{2+}, which replace Zn^{2+} ions in the ZnO lattice. With the addition of Ni dopants, the bandgap energy decreases due to the absorption of visible light, resulting from introducing defect states within the band structure. For biomolecule-capped ZnO: Ni QDs, a stronger absorption band was detected compared to uncapped ZnO: Ni QDs [38]. During encapsulation, the biomolecules (starch, glucose, sucrose) on the quantum dot surface likely modify the electronic environment of the QDs, resulting in increased absorption intensity. Similar effects were also observed for polymer-capped ZnO QDs.

The optical bandgap (Eg) values were determined using the Tauc plot method: $\alpha h\nu = A\,(h\nu - Eg)$ where α is the absorption coefficient, h is the photon energy, A is a constant, and $n = 1/2$ for direct bandgap materials [39]. The calculated bandgap energy values are presented in Table 1. The findings indicate that Ni doping reduces the bandgap energy of ZnO QDs from 3.37 eV (pure ZnO) to approximately 3.20 eV (ZnO: Ni). It is also noted that biomolecule capping further adjusts the bandgap due to surface modifications. The PL emission spectra of all samples are shown in Fig. 5. The emission peaks for ZnO: Ni QDs exhibited strong violet emission at approximately 380 nm, corresponding to near-band-edge excitonic (defect) recombination [40]. A defect was also associated with an emission peak around 470 nm due to trapping states created by Ni doping. These emissions show that Ni doping introduces shallow trap states within the bandgap, which enhances radiative recombination (see Fig. 6).

Distinct emission profiles were observed for the biomolecule-capped ZnO: Ni QDs. ZnO: Ni/Starch exhibited broad emission bands of violet-blue color roughly between 380 and 450 nm due to lower defect states resulting from improved capping. In this case, increased blue emission at 465 nm was observed due to stronger interactions between glucose molecules and the trap states on the QD surface. This study (ZnO: Ni/Sucrose) reports a broad emission from violet to near-red (~465–600 nm) due to complex trap-state recombination influenced by sucrose encapsulation. These behaviors are consistent with previously reported results for capped ZnO QDs, where biomolecular or polymeric surface modifications significantly influenced emission properties [41]. The optical behavior of Ni-doped and biomolecule-capped ZnO QDs can be attributed to the enhanced absorption of visible light due to photochemical reactions, which is improved when the bandgap energy is

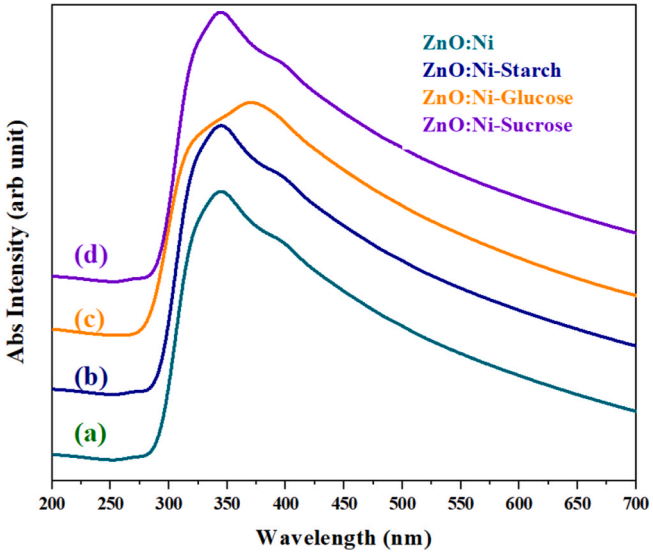


Fig. 4. UV absorption spectrum of (a) ZnO:Ni, (b) ZnO:Ni/Starch, (c) ZnO:Ni/Glucose and (d) ZnO:Ni/Sucrose QD samples.

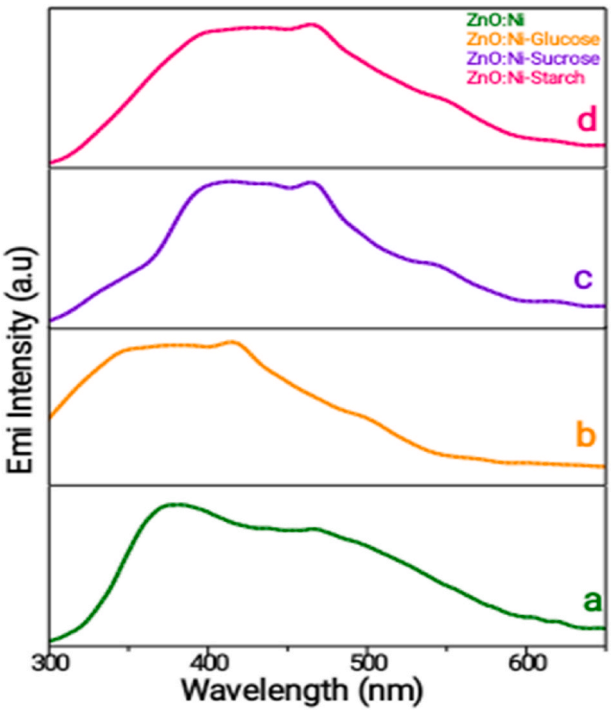


Fig. 5. PL emission spectrum of (a) ZnO:Ni, (b) ZnO:Ni/Starch, (c) ZnO:Ni/Glucose and (d) ZnO:Ni/Sucrose QD samples.

decreased via sp-d exchange interactions between conduction band electrons and localized d-electron states induced by Ni [42]. Non-radiative recombination paths caused by biomolecular capping through hydrogen bonding and electrostatic interactions with the surfaces of the nanoparticles are proposed to be reduced, leading to enhanced radiative emission.

3.4. Photoluminescence emission analysis

The PL Emission spectra of pure ZnO, Ni-doped ZnO (ZnO: Ni) quantum dots, and biomolecule-capped Ni-doped ZnO quantum dots (ZnO: Ni/Starch, ZnO: Ni/Glucose, and ZnO: Ni/Sucrose) were captured to study their electronic transitions and defect-related emissions [43]. The reincorporation mechanisms and the alteration of charge carrier and optical characteristics due to doping and capping were discussed within the scope of the available data from the PL spectra. For the ZnO: Ni QDs, a strong peak of violet emission (~380 nm) ascribed to the near-band-edge excitonic recombination of a free electron in the conduction band with a bound hole in the valence band was observed. Also recorded was a weaker blue emission peak (~470 nm), corresponding to defect states such as oxygen vacancies or zinc interstitials created after Ni doping [44]. These defect states introduce electron traps, enabling radiative recombination at lower energy levels [45]. Capped biomolecule composites of ZnO: Ni QDs displayed different PL features depending on the capping molecule. The emission profile of ZnO: Ni/Starch QDs was a wide violet-blue band (~380–450 nm), suggesting that starch molecules led to effective surface passivation by reducing non-radiative recombination pathways and improving the efficiency of radiative processes [46]. An intense blue emission at ~465 nm for ZnO: Ni/Glucose QDs suggested that glucose molecules interact robustly with surface trap states, stabilizing the defects and augmenting the defect-related emissions. Sucrose-capped QDs exhibited a broad near violet to red (~465–600 nm) emission spectrum, which is attributed to complex trap-state recombination, believed to be influenced by the sucrose encapsulation that introduces additional electronic interactions at the surface of the nanoparticles.

The PL behavior is divided into two distinct mechanisms: (1) near band edge emission at approximately ~380 nm, which is prominent in all samples due to excitonic recombination in the lattice of ZnO, and (2) defect-related emissions at ~470–600 nm originating from the trap states associated with oxygen vacancies, zinc interstitials, or other surface defects produced during the synthetic or doping processes. The surface defects on the QDs have varying electronic environments, which modify these emissions through passivation [47]. Glucose-capped and sucrose samples exhibited stronger interactions with surface defects than the starch-capped samples, leading to increased blue and red emissions. These observations are consistent with existing literature on ZnO nanoparticles, where violet emissions close to ~380 nm were linked to excitonic recombination. In comparison, blue emissions at approximately ~470 nm were associated with oxygen vacancies in the doped systems [48]. The observed broad multi-wavelength emissions for sucrose-capped samples align with those reported for polymer- or biomolecule-functionalized ZnO nanoparticles [1]. The incorporation of Ni doping produced shallow trap states within the bandgap, thereby enhancing defect-related emissions, while biomolecule capping mitigated non-radiative recombination processes to improve radiative efficiency. Such controllable PL behavior renders biomolecule-capped ZnO:

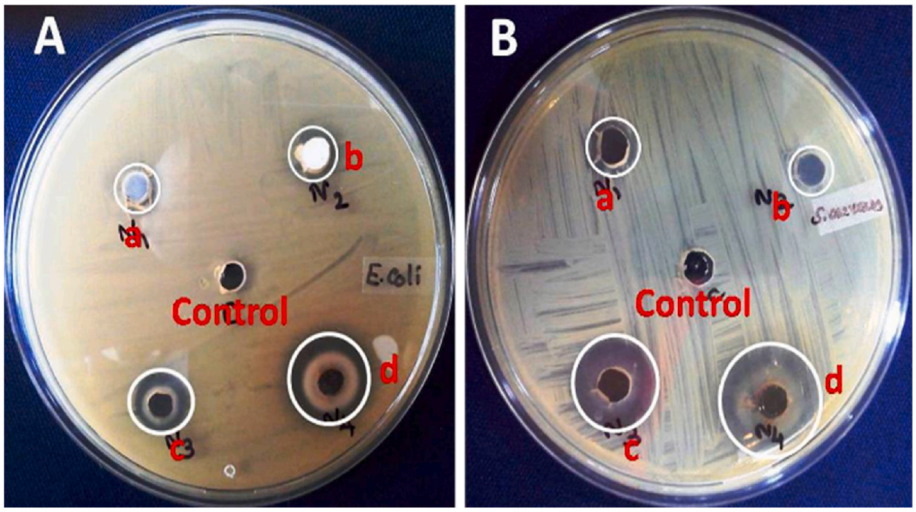


Fig. 6. Antibacterial activity of (center) control, (a) ZnO:Ni, (b) ZnO:Ni/Starch, (c) ZnO:Ni/Glucose and (d) ZnO:Ni/Sucrose QDs against *E. coli* (A) and *S. aureus* (B) after 24 h.

Ni QDs promising candidates for optoelectronic, bioimaging, and biosensing devices [49].

3.5. Antibacterial activity

The antibacterial characteristics of ZnO, Ni-doped ZnO (ZnO: Ni), and biomolecule-capped Ni-doped ZnO quantum dots (ZnO: Ni/starch, ZnO: Ni/glucose, ZnO: Ni/sucrose) were assessed against Escherichia coli (E. coli, Gram-negative) and Staphylococcus aureus (S. aureus, Gram-positive) using the disc diffusion method [50]. The findings indicated that biomolecule-capped ZnO: Ni QDs displayed superior antibacterial effects compared to uncapped ZnO: Ni QDs, with the ZnO: Ni/sucrose QDs showing the most significant inhibition zones for both bacterial strains [51]. This dominant effect was attributed to the smaller particle size (~10–20 nm), which increases the surface area-to-volume ratio, combined with the impact of biomolecule capping that amplifies interaction with bacterial membranes [52]. Among the capped samples, sucrose-capped ZnO: Ni QDs exhibited the most potent antibacterial effect due to a higher generation of reactive oxygen species (ROS) and strong binding to bacterial cell walls. The antibacterial function of ZnO-based QDs operates through a combination of mechanisms [53]. Firstly, the generation of ROS, such as hydroxyl radicals (-OH), superoxide anions (O_2^-), and hydrogen peroxide (H_2O_2), disrupts membranes and intracellular components, leading to bacterial cell death [54]. Secondly, the increased membrane permeability resulting from Zn^{2+} ions released from the nanoparticles interferes with metabolic processes and induces oxidative stress in the bacterial cells. Finally, damage to the bacterial cell wall due to the strong electrostatic forces between positively charged QDs and negatively charged bacterial membranes results in cytoplasm leakage [55]. All these mechanisms contribute to the broad-spectrum antibacterial activity observed in this study.

Furthermore, S. aureus showed more excellent resistance than E. coli, indicating the antibacterial activity was more pronounced against S. aureus [56] (see Fig. 7). This can be attributed to differences in their cell wall structures. As a Gram-positive bacterium, S. aureus has a thick peptidoglycan layer, allowing Zn^{2+} ions and ROS to interact effectively. In contrast, E. coli, being Gram-negative, has an outer membrane composed of lipopolysaccharides that protect against nanoparticle invasion [57]. The capping with curcumin and albumin enhances the antibacterial activity of ZnO: Ni QDs by stabilizing the nanoparticles to prevent aggregation and adding functional groups that improve attachment to bacterial surfaces [58]. Moreover, capping modifies the surface defects on the nanoparticles, increasing ROS generation efficiency. Consequently, the sucrose-capped ZnO: Ni QDs demonstrated the highest antibacterial activity due to their stable encapsulation layer, which boosted ROS production and interaction with bacterial membranes [58]. This aligns with previous research indicating that smaller-sized (<20 nm) particles have enhanced antibacterial activity due to increased surface area. Additionally, biomolecule-capped nanoparticles are known to exhibit improved antibacterial activity, biocompatibility, and stability due to surface modifications (Fig. 8). The results further corroborate what has been established regarding the antibacterial effects of ZnO nanoparticles, which are known to result from the interplay of ROS production, cell wall disintegration, nanoparticle cellular internalization, and toxic levels of zinc ions [59]. Given the high antimicrobial activity of biomolecule-capped ZnO: Ni QDs, they have emerged as promising candidates for application in various biomedical fields, including wound dressing materials, medical implant coatings, food packaging, and water disinfection. These findings also underscore the importance of doping and capping techniques in enhancing the antimicrobial efficacy of nanomaterials. (see Table 2)

4. Conclusion

This research successfully achieved the green synthesis of pure ZnO, Ni-doped ZnO (ZnO: Ni), and biomolecule-capped ZnO: Ni quantum dots (ZnO: Ni/Starch, ZnO: Ni/Glucose, and ZnO: Ni/Sucrose). The properties of the as-synthesized quantum dots regarding structure, morphology, optics, and antimicrobial action were thoroughly evaluated. XRD patterns confirmed the incorporation of Ni into ZnO QDs, resulting in cubic *hexagonal micrometric crystals with an average crystallite size of approximately 12 nm. TEM images displayed spherical uncapped QDs with diameters under 10 nm and biomolecule-capped QDs measuring 10–20 nm due to starch, glucose, and sucrose encapsulation. Optical studies indicated that Ni-doped samples captured the absorption peak (sp-d exchange interactions) at approximately 343 nm and further absorption due to biomolecule capping. PL analysis established excitonic recombination at the near band edge (~380 nm) and defect emissions from excitation radiation between ~470 and 600 nm, significantly influenced by the dopant type and capping agent. Sucrose-capped ZnO: Ni QDs exhibited the most complex trap-state recombination and the broadest reported emission spectrum.

The antibacterial efficacy of the produced quantum dots (QDs) was

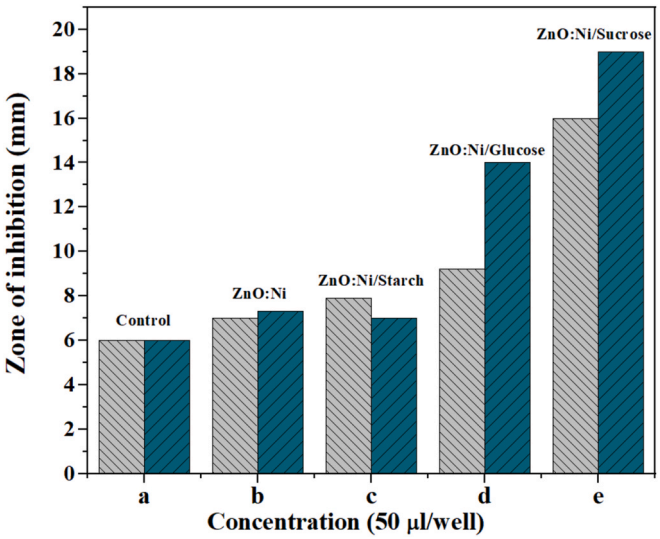


Fig. 7. Comparison of antibacterial activity of (a) Control, (b) ZnO:Ni, (c) ZnO: Ni/Starch, (d) ZnO:Ni/Glucose and (e) ZnO:Ni/Sucrose QDs against *E. coli* and *S. aureus* after 24 h.

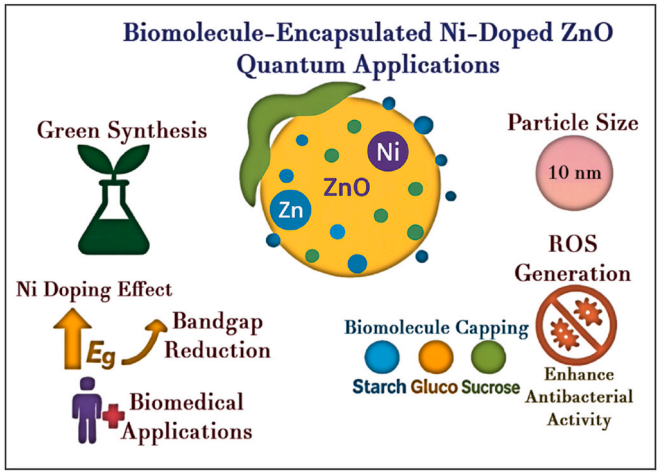


Fig. 8. Schematic summary of green synthesis and bio/multi-function of biomolecule-capped Ni-doped ZnO quantum dots, where Ni doping and biomolecule capping can adjust the particle size, bandgap, and antibacterial activity by promoting ROS production. (For interpretation of the references to color in this figure legend, the reader is referred to the Web version of this article.)

tested on both Escherichia coli (E. coli, Gram-negative) and Staphylococcus aureus (S. aureus, Gram-positive) bacteria. The biomolecule-bound ZnO: Ni QDs outperformed uncapped ones, with the sucrose-capped samples demonstrating the highest performance. The believed causes of the increased activity include enhanced reactive oxygen species (ROS) production, zinc ion release, effective membrane disruption in the bacteria, smaller particle size, and stable biomolecule encapsulation. The mechanism of action was found to be more effective with S. aureus due to its less complex cell wall structure than E. coli, which has an additional outer membrane. Overall, the results validate the potential of green-synthesized, biomolecule-capped Ni-doped ZnO quantum dots for use in biomedical devices, such as antibacterial coatings, wound healing materials, and medical implants. Ni doping and natural biomolecule capping enhance the structural stability and optical properties of the ZnO QDs, enabling higher antimicrobial efficacy. Further research is required to ascertain these materials' durability, cytotoxicity, and practicality for medical and environmental applications.

CRediT authorship contribution statement

R. Anithadevi: Formal analysis, Data curation, Conceptualization. **J.C. Kannan:** Writing – original draft, Investigation, Formal analysis, Data curation, Conceptualization. **P. Sangeetha:** Writing – original draft, Methodology, Investigation. **M. Thirumoorthy:** Writing – original draft, Validation, Investigation. **A. Panneerselvam:** Writing – original draft, Supervision, Investigation, Formal analysis. **T. Baranidharan:** Writing – original draft, Supervision, Investigation. **P. Periasamy:** Visualization, Supervision, Methodology, Formal analysis. **S. Satheeskumar:** Writing – review & editing, Writing – original draft, Supervision, Data curation, Conceptualization.

Funding

There was no funding from any agency.

Declaration of competing interest

The authors declare that they have no known competing financial interests or personal relationships that could have appeared to influence the work reported in this paper.

Acknowledgment

We sincerely thank Dr. R. Gopalakrishnan, Principal of K.S. Rangasamy College of Technology, Tiruchengode, for his unwavering encouragement and support throughout this work.

Data availability

Data will be made available on request.

References

[1] S. Raha, M. Ahmaruzzaman, ZnO nanostructured materials and their potential applications: progress, challenges and perspectives, Nanoscale Adv. 4 (8) (Apr. 2022) 1868–1925, https://doi.org/10.1039/D1NA00880C.
[2] Y. Sun, W. Zhang, Q. Li, H. Liu, X. Wang, Preparations and applications of zinc oxide based photocatalytic materials, Adv. Sens. Energy Mater. 2 (3) (Sep. 2023) 100069, https://doi.org/10.1016/J.ASEMS.2023.100069.
[3] Preeti, V.S. Radhakrishnan, S. Mukherjee, S. Mukherjee, S.P. Singh, T. Prasad, ZnO quantum dots: broad spectrum microbicidal agent against multidrug resistant pathogens E. coli and C. albicans, Front. Nanotechnol. 2 (Nov. 2020) 576342, https://doi.org/10.3389/FNANO.2020.576342/BIBTEX.
[4] I. Ahmad, M.A. Aftab, A. Fatima, S.D. Mekkey, S. Melhi, S. Ikram, A comprehensive review on the advancement of transition metals incorporated on functional magnetic nanocomposites for the catalytic reduction and photocatalytic degradation of organic pollutants, Coord. Chem. Rev. 514 (Sep. 2024) 215904, https://doi.org/10.1016/J.CCR.2024.215904.
[5] M.Y. Ali, M.K.R. Khan, A.M.M.T. Karim, M.M. Rahman, M. Kamruzzaman, Effect of Ni doping on structure, morphology and opto-transport properties of spray pyrolised ZnO nano-fiber, Heliyon 6 (3) (Mar. 2020) e03588, https://doi.org/10.1016/J.HELIYON.2020.E03588.
[6] H. Ali, et al., Influence of nickel doping on the energy band gap, luminescence, and magnetic order of spray deposited nanostructured ZnO thin films, J. Alloys Compd. 816 (Mar) (2020), https://doi.org/10.1016/J.JALLCOM.2019.152538.
[7] F.C. C, K. T, Advances in stabilization of metallic nanoparticle with biosurfactants-a review on current trends, Heliyon 10 (9) (May 2024) e29773, https://doi.org/10.1016/J.HELIYON.2024.E29773.
[8] Z. Montaseri, A.M. Tamaddon, M.J. Raee, F. Farvadi, Exploring the effects of various capping agents on zinc sulfide quantum dot characteristics and in-Vitro fate, ChemistryOpen 12 (10) (Oct. 2023) e202300094, https://doi.org/10.1002/OPEN.202300094.
[9] I.H. Ifijen, M. Maliki, B. Anegbe, Synthesis, photocatalytic degradation and antibacterial properties of selenium or silver doped zinc oxide nanoparticles: a detailed review, OpenNano 8 (Nov. 2022) 100082, https://doi.org/10.1016/J.ONANO.2022.100082.
[10] W.J. Qin, J. Sun, J. Yang, X.W. Du, Control of Cu-doping and optical properties of ZnO quantum dots by laser ablation of composite targets, Mater. Chem. Phys. 130 (1–2) (Oct. 2011) 425–430, https://doi.org/10.1016/J.MATCHEMPHYS.2011.07.001.
[11] A. Sirelkhatim, et al., Review on zinc oxide nanoparticles: antibacterial activity and toxicity mechanism, Nano-Micro Lett. 7 (3) (Apr. 2015) 219–242, https://doi.org/10.1007/S40820-015-0040-X/TABLES/2.
[12] G. Srinet, R. Kumar, V. Sajal, Effects of Ni doping on structural, optical and dielectric properties of ZnO, Ceram. Int. 39 (7) (Sep. 2013) 7557–7561, https://doi.org/10.1016/J.CERAMINT.2013.03.008.
[13] R. Zhang, et al., Enhanced photodynamic therapy efficacy of Ni-doped/oxygen vacancy double-defect Ni-ZnO@C photosensitizer in bacteria-infected wounds based on ROS damage and ATP synthesis inhibition, J. Mater. Sci. Technol. 192 (Sep. 2024) 173–189, https://doi.org/10.1016/J.JMST.2024.01.018.
[14] A.K. Sidhu, N. Verma, P. Kaushal, Role of biogenic capping agents in the synthesis of metallic nanoparticles and evaluation of their therapeutic potential, Front. Nanotechnol. 3 (Jan. 2022) 801620, https://doi.org/10.3389/FNANO.2021.801620/PDF.
[15] B. Mohapatra, S. Mohapatra, N. Sharma, Biosynthesized Ag–ZnO nanohybrids exhibit strong antibacterial activity by inducing oxidative stress, Ceram. Int. 49 (12) (Jun. 2023) 20218–20233, https://doi.org/10.1016/J.CERAMINT.2023.03.146.
[16] H.J. Kim, S.H. Lee, D. Jeon, S.N. Lee, High-performance Sol–gel-derived CNT-ZnO nanocomposite-based photodetectors with controlled surface wrinkles, Materials 17 (21) (Nov. 2024) 5325, https://doi.org/10.3390/MA17215325/S1.
[17] O. Akhavan, E. Ghaderi, A. Esfandiar, Wrapping bacteria by graphene nanosheets for isolation from environment, reactivation by sonication, and inactivation by near-infrared irradiation, J. Phys. Chem. B 115 (19) (May 2011) 6279–6288, https://doi.org/10.1021/JP200686K/ASSET/IMAGES/MEDIUM/JP-2011-00686K_0008.GIF.
[18] K. Liu, et al., MXene-loaded multifunctional nanoparticles with on-demand controlled antimicrobial and antioxidant capacity for multi-modal treating bacterial prostatitis, Biomaterials 320 (Sep. 2025) 123234, https://doi.org/10.1016/J.BIOMATERIALS.2025.123234.
[19] S. Abou Zeid, et al., Antibacterial and photocatalytic properties of ZnO nanostructure decorated coatings, Coatings 14 (1) (Dec. 2023) 41, https://doi.org/10.3390/COATINGS14010041, 2024, Vol. 14, Page 41.
[20] S.V. Gudkov, D.E. Burmistrov, D.A. Serov, M.B. Rebezov, A.A. Semenova, A. B. Lisitsyn, A mini review of antibacterial properties of ZnO nanoparticles, Front. Physiol. 9 (Mar. 2021) 641481, https://doi.org/10.3389/FPHY.2021.641481/PDF.
[21] M. Pandey, et al., Targeted and enhanced antimicrobial inhibition of mesoporous ZnO-Ag2O/Ag, ZnO-CuO, and ZnO-SnO2Composite nanoparticles, ACS Omega 6 (47) (Nov. 2021) 31615–31631, https://doi.org/10.1021/ACSOMEGA.1C04139/ASSET/IMAGES/LARGE/AO1C04139_0011.JPEG.
[22] H. Mohammed, et al., Antimicrobial mechanisms and effectiveness of graphene and graphene-functionalized biomaterials. A scope review, Front. Bioeng. Biotechnol. 8 (May 2020) 498689, https://doi.org/10.3389/FBIOE.2020.00465/PDF.
[23] A. Badoni, J. Prakash, Noble metal nanoparticles and graphene oxide based hybrid nanostructures for antibacterial applications: recent advances, synergistic antibacterial activities, and mechanistic approaches, Micro. Nano. Eng. 22 (Mar. 2024) 100239, https://doi.org/10.1016/J.MNE.2024.100239.
[24] R. Ahmadi, R. Fattahi Nafchi, P. Sangpour, M. Bagheri, E. Badiei, A comparative study: green synthesis and evaluation of ZnO-GO and ZnO-RGO nanocomposites for antibacterial applications, Mater. Sci. Eng. B 294 (Aug. 2023) 116555, https://doi.org/10.1016/J.MSEB.2023.116555.
[25] K. Rasool, M. Helal, A. Ali, C.E. Ren, Y. Gogotsi, K.A. Mahmoud, Antibacterial activity of Ti_3C_2Tx MXene, ACS Nano 10 (3) (Mar. 2016) 3674–3684, https://doi.org/10.1021/ACSNANO.6B00181.
[26] M. Achehboune, M. Khenfouch, I. Boukhoubza, B. Mothudi, I. Zorkani, A. Jorio, Study on the effect of Er dopant on the structural properties of ZnO nanorods synthesized via hydrothermal method, J. Phys. Conf. Ser. 1292 (1) (Sep. 2019), https://doi.org/10.1088/1742-6596/1292/1/012020.
[27] D. Destalina, F. Mujtahid, I. Mutmainna, D. Tahir, P.L. Gareso, XRD structure study on nickel doped zinc oxide nanoparticles synthesized by coprecipitation method, Indones. Phys. Rev. 5 (3) (Aug. 2022) 188–196, https://doi.org/10.29303/IPR.V5I3.179.
[28] P.S. Kumar, et al., Biodegradability study and pH influence on growth and orientation of ZnO nanorods via aqueous solution process, Appl. Surf. Sci. 258 (18) (Jul. 2012) 6765–6771, https://doi.org/10.1016/J.APSUSC.2012.03.051.

[29] M.I. Zakirov, M.P. Semen'ko, O.A. Korotchenkov, A simple sonochemical synthesis of nanosized ZnO from zinc acetate and sodium hydroxide, J. Nano- Electron. Phys. 10 (5) (2018), https://doi.org/10.21272/JNEP.10(5).05023.
[30] A. Mokhles Gerami, M. Vaez-Zadeh, A numerical study on magnetic and structural properties of Ni-Doped ZnO nanoparticles at extremely low temperatures, J. Supercond. Nov. Magnetism 29 (5) (May 2016) 1295–1302, https://doi.org/10.1007/S10948-016-3411-8/METRICS.
[31] C. Zegadi, et al., Influence of Sn low doping on the morphological, structural and optical properties of ZnO films deposited by sol gel dip-coating, Adv. Mater. Phys. Chem. 4 (5) (May 2014) 93–104, https://doi.org/10.4236/AMPC.2014.45012.
[32] P. Singh, R.K. Singh, R. Kumar, Journey of ZnO quantum dots from undoped to rare-earth and transition metal-doped and their applications, RSC Adv. 11 (4) (Jan. 2021) 2512–2545, https://doi.org/10.1039/D0RA08670C.
[33] I.A. Vagena, et al., Functionalized ZnO-Based nanocomposites for diverse biological applications: current trends and future perspectives, Nanomaterials 14 (5) (Feb. 2024) 397, https://doi.org/10.3390/NANO14050397, 2024, Vol. 14, Page 397.
[34] C. Chen, D.Y.W. Ng, T. Weil, Polymer bioconjugates: modern design concepts toward precision hybrid materials, Prog. Polym. Sci. 105 (Jun. 2020) 101241, https://doi.org/10.1016/J.PROGPOLYMSCI.2020.101241.
[35] S. Kundu, A. Patra, Nanoscale strategies for light harvesting, Chem. Rev. 117 (2) (Jan. 2017) 712–757, https://doi.org/10.1021/ACS.CHEMREV.6B00036/ASSET/IMAGES/MEDIUM/CR-2016-000363_0033.GIF.
[36] M.T. Islam, A. Dominguez, B. Alvarado-Tenorio, R.A. Bernal, M.O. Montes, J. C. Noveron, Sucrose-mediated fast synthesis of zinc oxide nanoparticles for the photocatalytic degradation of organic pollutants in water, ACS Omega 4 (4) (Apr. 2019) 6560–6572, https://doi.org/10.1021/ACSOMEGA.9B00023/ASSET/IMAGES/LARGE/AO-2019-000238_0005.JPEG.
[37] A.K. Verma, G.B.V.S. Lakshmi, T.K. Dhiman, S.Z.H. Hashmi, A. Kumar, P. R. Solanki, Optical tuning of polymer functionalized zinc oxide quantum dots as a selective probe for the detection of antibiotics, Sci. Rep. 15 (1) (Jan. 2025) 1–12, https://doi.org/10.1038/s41598-024-62827-0, 2024 151.
[38] C. Jing, Y. Jiang, W. Bai, J. Chu, A. Liu, Synthesis of Mn-doped ZnO diluted magnetic semiconductors in the presence of ethyl acetoacetate under solvothermal conditions, J. Magn. Magn Mater. 322 (16) (Aug. 2010) 2395–2400, https://doi.org/10.1016/J.JMMM.2010.02.044.
[39] A. Dolgonos, T.O. Mason, K.R. Poeppelmeier, Direct optical band gap measurement in polycrystalline semiconductors: a critical look at the Tauc method, J. Solid State Chem. 240 (Aug. 2016) 43–48, https://doi.org/10.1016/J.JSSC.2016.05.010.
[40] S.K. Mishra, R.K. Srivastava, S.G. Prakash, ZnO nanoparticles: structural, optical and photoconductivity characteristics, J. Alloys Compd. 539 (Oct. 2012) 1–6, https://doi.org/10.1016/J.JALLCOM.2012.06.024.
[41] G. Saber, A. El-Dissouky, G. Badie, S. Ebrahim, A. Shokry, Capped ZnO quantum dots with a tunable photoluminescence for acetone detection, RSC Adv. 13 (24) (Jun. 2023) 16453–16470, https://doi.org/10.1039/D3RA00491K.
[42] I. Virt, P. Potera, R. Gamernyk, C. Bogumił, "Structural and optical properties of Ni-Doped zno thin films as tco material. Fabricated by Pulsed Laser Deposition Method, 2023, https://doi.org/10.2139/SSRN.4606465.
[43] M. Silambarasan, S. Saravanan, N. Ohtani, T. Soga, Structural and photoluminescence studies of Ni-doped ZnO nanoparticles synthesized by solution combustion method, Palliat. Support Care 1584 (1) (Jan. 2014), https://doi.org/10.1557/OPL.2014.187.
[44] H. Zeng, G. Duan, Y. Li, S. Yang, X. Xu, W. Cai, Blue luminescence of ZnO nanoparticles based on non-equilibrium processes: defect origins and emission controls, Adv. Funct. Mater. 20 (4) (Feb. 2010) 561–572, https://doi.org/10.1002/ADFM.200901884.
[45] B. Khodadadi, M. Bordbar, A. Yeganeh-Faal, Optical, structural, and photocatalytic properties of Cd-doped ZnO powders prepared via sol–gel method, J. Sol. Gel Sci. Technol. 77 (3) (Oct. 2015) 521–527, https://doi.org/10.1007/S10971-015-3877-Z, 2015 773.
[46] K. Vidhya, M. Saravanan, G. Bhoopathi, V.P. Devarajan, S. Subanya, Structural and optical characterization of pure and starch-capped ZnO quantum dots and their photocatalytic activity, Appl. Nanosci. 5 (2) (Feb. 2015) 235–243, https://doi.org/10.1007/S13204-014-0312-7.
[47] A. Chahboun, A.G. Rolo, S.A. Filonovich, M.J.M. Gomes, Factors influencing the passivation of CdS quantum dots embedded in silica glass, Sol. Energy Mater. Sol. Cells 90 (10) (Jun. 2006) 1413–1419, https://doi.org/10.1016/J.SOLMAT.2005.10.006.
[48] S. Faisal, et al., Green synthesis of zinc oxide (ZnO) nanoparticles using aqueous fruit extracts of myristica fragrans: their characterizations and biological and environmental applications, ACS Omega 6 (14) (Apr. 2021) 9709–9722, https://doi.org/10.1021/ACSOMEGA.1C00310/ASSET/IMAGES/MEDIUM/AO1C00310_M014.GIF.
[49] M.R.C. Sytu, J.I. Hahm, Principles and applications of ZnO nanomaterials in optical biosensors and ZnO nanomaterial-enhanced biodetection, Biosens 14 (10) (Oct. 2024) 480, https://doi.org/10.3390/BIOS14100480, 2024, Vol. 14, Page 480.
[50] A. Naskar, S. Lee, K.S. Kim, Antibacterial potential of Ni-doped zinc oxide nanostructure: comparatively more effective against Gram-negative bacteria including multi-drug resistant strains, RSC Adv. 10 (3) (Jan. 2020) 1232–1242, https://doi.org/10.1039/C9RA09512H.
[51] Y. Li, S. Xie, D. Xu, G. Shu, X. Wang, Antibacterial activity of ZnO quantum dots and its protective effects of chicks infected with Salmonella pullorum, Nanotechnology 32 (50) (Dec. 2021), https://doi.org/10.1088/1361-6528/AC2846.
[52] M. Godoy-Gallardo, et al., Antibacterial approaches in tissue engineering using metal ions and nanoparticles: from mechanisms to applications, Bioact. Mater. 6 (12) (Dec. 2021) 4470–4490, https://doi.org/10.1016/J.BIOACTMAT.2021.04.033.
[53] R. Krishnamoorthy, et al., Antibacterial mechanisms of zinc oxide nanoparticle against bacterial food pathogens resistant to beta-lactam antibiotics, Molecules 27 (8) (Apr. 2022) 2489, https://doi.org/10.3390/MOLECULES27082489.
[54] C.A. Juan, J.M.P. de la Lastra, F.J. Plou, E. Pérez-Lebeña, The chemistry of Reactive Oxygen Species (ROS) revisited: outlining their role in biological macromolecules (DNA, lipids and proteins) and induced pathologies, Int. J. Mol. Sci. 22 (9) (2021) 4642, https://doi.org/10.3390/IJMS22094642.
[55] N. Mammari, E. Lamouroux, A. Boudier, R.E. Duval, Current knowledge on the oxidative-stress-mediated antimicrobial properties of metal-based nanoparticles, Microorganisms 10 (2) (Feb. 2022) 437, https://doi.org/10.3390/MICROORGANISMS10020437.
[56] D.P. Tamboli, D.S. Lee, Mechanistic antimicrobial approach of extracellularly synthesized silver nanoparticles against gram positive and gram negative bacteria, J. Hazard. Mater. 260 (Sep. 2013) 878–884, https://doi.org/10.1016/J.JHAZMAT.2013.06.003.
[57] D. Brdová, T. Ruml, J. Viktorová, Mechanism of staphylococcal resistance to clinically relevant antibiotics, Drug Resist. Updates 77 (Nov. 2024) 101147, https://doi.org/10.1016/J.DRUP.2024.101147.
[58] J. Shen, et al., How muscles recover from paresis and atrophy after intramuscular injection of botulinum toxin A: study in juvenile rats, J. Orthop. Res. 24 (5) (May 2006) 1128–1135, https://doi.org/10.1002/JOR.20131.
[59] T. Xia, M. Kovochich, M. Liong, J.I. Zink, A.E. Nel, Cationic polystyrene nanosphere toxicity depends on cell-specific endocytic and mitochondrial injury pathways, ACS Nano 2 (1) (Jan. 2008) 85–96, https://doi.org/10.1021/NN700256C/SUPPL_FILE/NN700256C-FILE002.PDF.